Draft version January 29, 2018
Preprint typeset using LaTeX style emulateapj v. 12/16/11

ALMA DETECTION OF EXTENDED [CII] EMISSION IN HIMIKO AT Z=6.6

S. Carniani[1,2], R. Maiolino[1,2], R. Smit[1,2], and R. Amorín[1,2]

(Received Dec 4, 2017; Revised; Accepted January 29, 2018)
Draft version January 29, 2018

ABSTRACT

Himiko is one of the most luminous Lyα emitters at $z = 6.595$. It has three star forming clumps detected in the rest-frame UV, with a total SFR = 20 $M_\odot$/yr. We report the ALMA detection of the [CII]158μm line emission in this galaxy with a significance of 8σ. The total [CII] luminosity ($L_{[CII]}$=1.2 $\times$ 10^8 $L_\odot$) is fully consistent with the local $L_{[CII]}$-SFR relation. The ALMA high-angular resolution reveals that the [CII] emission is made of two distinct components. The brightest [CII] clump is extended over 4 kpc and is located on the peak of the Lyα nebula, which is spatially offset by 1 kpc relative to the brightest UV clump. The second [CII] component is spatially unresolved (size <2 kpc) and coincident with one of the three UV clumps. While the latter component is consitent with the local $L_{[CII]}$-SFR relation, the other components are scattered above and below the local relation. We shortly discuss the possible origin of the [CII] components and their relation with the star forming clumps traced by the UV emission.

Subject headings: galaxies: formation — galaxies: high-redshift — infrared: ISM — galaxies: evolution

1. INTRODUCTION

One of the key science goals of the Atacama Large Millimitre/submillimetre Array (ALMA) is the detection and investigation of star-forming galaxies in the early Universe through the observations of the far-infrared (FIR) lines. In particular, ALMA observations of the strongest FIR lines, such as the [CII]158μm and [OIII]88μm, allow us to probe the properties of the interstellar medium (ISM) in galaxies at $z > 6$ (e.g. Maiolino et al. 2015; Pentericci et al. 2016; Carniani et al. 2017a; Inoue et al. 2016; Matthee et al. 2017; Smit et al. 2017), which are responsible for cosmic reionisation.

The [CII] ($^2P_{3/2} \rightarrow {}^2P_{1/2}$) transition at 157.74 μm, whose emissivity is mainly driven by the collisional excitation mechanism, is one of the dominant coolants of the neutral and partly ionised ISM. Furthermore, [CII] is directly correlated to star-formation, since its emission can be excited by the UV radiation field of young stars in photodissociation regions. This transition can therefore be used as tracer of on-going star-formation in local and distant star-forming galaxies (e.g. De Looze et al. 2014; Vallini et al. 2015; Herrera-Camus et al. 2015), except for ultra-luminous systems (Díaz-Santos et al. 2013; Smith et al. 2017; Kapala et al. 2015)

In the last five years ALMA observations targeting the [CII] line emission in "normal" star-forming galaxies $z > 6$ (with SFR = 3-100 $M_\odot$/yr) have yielded a variety of results (Ouchi et al. 2013; Ota et al. 2014; Willott et al. 2015; Maiolino et al. 2015; Pentericci et al. 2016; Bradač et al. 2016; Knudsen et al. 2016; Matthee et al. 2017; Smit et al. 2017). The $L_{[CII]}$-SFR relation observed in these high-z systems seems to have an intrinsic dispersion larger than that observed in the local Universe, which probably results from the wide range of global properties characterising primeval galaxies (Vallini et al. 2015; Matthee et al. 2017; Lagache et al. 2017; Carniani et al. 2017b). The properties of the [CII] emission are even more puzzling in luminous Lyα emitters (LAEs) whose detections or upper limits (Walter et al. 2012; Ouchi et al. 2013; Ota et al. 2014; Willott et al. 2015; Schaerer et al. 2015) place these sources below the $L_{[CII]}$-SFR relation found in the local Universe (De Looze et al. 2014). So far, the only LAE having a [CII] emission consistent with the local relation is CR7 at $z \sim 7$ (Matthee et al. 2017). Simulations and models have attempted to explain the discrepancy with the local relation by taking into account the low metal content in high-z galaxies, the excitation by the CMB radiation, and the effect of galactic outflows expelling large amounts of gas (Vallini et al. 2013, 2015; Pallottini et al. 2017a,b).

In this letter, we re-analyse archival ALMA [CII] observations of Himiko, one of the most famous LAE, at $z_{Ly\alpha} \sim 6.595$ (Ouchi et al. 2009, 2013; Zabl et al. 2015). HST observations with WFC3 in bands J_{125} and H_{160} (rest-frame UV at $z \sim 6.595$) show that Himiko comprises of three bright clumps (Figure 1). Its Lyα nebula extends over 17 kpc embedding all the tree clumps, but its peak is located between clumps A and B (Ouchi et al. 2013). The first ALMA observations aimed at detecting [CII] emission in Himiko system were obtained in Cycle 0 and presented in Ouchi et al. (2013), who reported a non detection for this galaxy placing an upper limit for the [CII] luminosity at $L_{[CII]} < 5.4 \times 10^7$ $L_\odot$. Himiko was also observed with ALMA in Cycle 1 but the analysis of these new observations have not been published so far.

In this paper we present an analysis of both Cycle-0 and Cycle-1 data. When combined together, we show that such data present a clear detection of [CII] with a luminosity expected by the local [CII]-SFR relation, and also present a clumpy morphology relative to the UV distribution.

Throughout this paper we adopt the standard cosmological parameters $H_0 = 70$ km s^{-1} Mpc^{-1} , $\Omega_M = 0.30$,

sc888@mrao.cam.ac.uk
[1] Cavendish Laboratory, University of Cambridge, 19 J. J. Thomson Ave., Cambridge CB3 0HE, UK
[2] Kavli Institute for Cosmology, University of Cambridge, Madingley Road, Cambridge CB3 0HA, UK

$\Omega_\Lambda = 0.70$. Magnitude are given in the AB system.

2. OBSERVATION AND DATA REDUCTION

Himiko was observed with ALMA in band 6 in July 2012 and July 2015 as part of the programs #2011.0.00115.S (Cycle 0) and #2012.1.00033.S (Cycle 1). The former program was carried out by using a semi-compact array configuration with a maximum baseline length of 440 m. An extended-array configuration was instead used for Cycle-1 observations, with baseline lengths up to 1600 m. Both observations were performed in frequency division mode with a total bandwidth of 7.5 GHz and a spectral resolution of 0.488 kHz (∼0.5 km/s).

The two datasets have been calibrated by using the standard scripts for ALMA data-reduction.We used the software CASA (McMullin et al. 2007) version 3.4.0 and 4.7.2 respectively for the two datasets. For each dataset we have generated the continuum map and cubes by using the CASA task CLEAN with a natural weighting. The resulting sensitivities and angular resolution are listed in Table 1. We note that the sensitivities and angular resolution achieved in Cycle-0 images are in agreement with those presented by Ouchi et al. (2013).

We have also combined the observations of both programs to obtain maps and cubes with higher sensitivity. The imaging of the combined dataset has been performed with a natural weighting, achieving a continuum sensitivity of 9 μJy/beam and an angular resolution of $\sim 0.30''$. To optimise the signal-to-nose ratio (S/N) of the [CII] detection, we have produced a spatially smoothed cube using a uv tapering of $0.2''$ so to recover the spatially extended emission. We report the properties of combined and smoothed images in Table 1.

We have registered the ALMA and HST data by matching ALMA calibrator and foreground sources to the GAIA Data Release 1 catalogue (Gaia Collaboration et al. 2016).

3. RESULTS

3.1. *Continuum emission at 158μm*

The dust continuum emission at 158μm is not detected, indicating a low dust mass content, as already discussed by Walter et al. (2012), Ouchi et al. (2013), and Ota et al. (2014). We estimate a 3σ upper limit on the continuum emission $S_{158\mu m} < 27$ μJy that results into a infrared luminosity $L_{IR} < 3 \times 10^{10}$ $L_\odot$, if assuming grey-body emission with a dust temperature of 35 K and a spectral emissivity index of 1.5 (Ota et al. 2014; Schaerer et al. 2015; Willott et al. 2015) and correcting for the effect of the CMB (da Cunha et al. 2013; Ota et al. 2014). Following the $L_{IR} - SFR_{IR}$ relation presented in Kennicutt & Evans (2012), the L_{IR} translates into a 3σ upper limit on the dust obscured $SFR_{IR} < 4$ $M_\odot$/yr. We note that such upper limit on SFR_{IR} is about four times lower than the total SFR_{UV} inferred from the rest-frame UV emission (see Table 2), indicating that most of the star formation is unobscured by dust.

3.2. *[CII] line emission*

We detect an emission line consistent with the [CII] emission at the redshift and at the location of Himiko in the combined uv-tapered ALMA cube. Figure 1a shows the map of the line extracted with a spectral width of 270 km/s and centred at -185 km/s relative to the $z_{Ly\alpha}$. The peak of the [CII] emission has a significance of 5.5σ and is located between the UV clumps A and B. However, the [CII] emission is spatially resolved, hence the significance of the total emission is higher than the peak flux in the map and specifically, as we will see below, the total significance is $\sim 8\sigma$. The distribution of the [CII] emission, estimated by using CASA's IMFIT task, has a beam-deconvolved size of $(0.7 \pm 0.2)'' \times (0.3 \pm 0.2)''$ embedding both UV clumps A and B.

The reliability of the [CII] detection is also supported by the fact that the line is marginally detected at the same location in the two individual datasets. More specifically, in the Cycle-0 data the peak of the [CII] emission is detected with a flux level $S\Delta v = 112 \pm 26$ mJy km/s (S/N=4.2) consistent with the value observed in the combined cube. The peak of the [CII] emission is only marginally detected with a $S\Delta v = 68 \pm 22$ mJy km/s (S/N=3.2) in the Cycle-1 observations. The lower significance in the Cycle-1 data is due to the high angular resolution of these data Indeed, although the Cycle-1 dataset has a sensitivity higher than that of Cycle-0, the diffuse emission is resolved out in the extended-array configuration observations and $\sim 40\%$ of the total [CII] emission is missed. A similar scenario has already been reported by Carniani et al. (2017a) for the $z = 7$ star-forming galaxy BDF-3299, where the bulk of the emission is ascribed diffuse gas extended on scales larger than 1 kpc and the new high-angular resolution observations have revealed only $\sim 30\%$ of the total [CII] emission.

Since the emission is resolved, we extract the [CII] spectrum over a region within the 2σ [CII] contours. The resulting spectrum, with a spectral rebinning of 40 km/s, is presented in Figure 1b, together with the optical spectrum of the Lyα line obtained from X-shooter observations (Zabl et al. 2015). The line is offset by -145±15 km/s relative to the $z_{Ly\alpha}$ and has a line width of 130±30 km/s. The velocity offsets between Lyα and [CII] emission is similar to those estimated in other high-z [CII]-emitting sources observed with ALMA (Maiolino et al. 2015; Pentericci et al. 2016; Matthee et al. 2017). While the [CII] line is a good tracer of the systemic velocity of galaxies in the early Universe, the Lyα profile is affected by intergalactic medium (IGM) absorption; galactic outflows can also shift the peak of the line by up to few hundred km/s. Zabl et al. (2015) discuss that the strong blue asymmetry of the Lyα profile is likely associated with the ISM/IGM absorption and, therefore, its centroid/peak results into an apparent redshift slightly higher than the systemic systemic redshift estimated from [CII], but fully consistent once the Lyα asymmetry is taken into account.

The integrated intensity of the [CII] line is $S_{[CII]}\Delta v = 108 \pm 12$ mJy km/s. The resulting [CII] luminosity $L_{[CII]} = (1.2 \pm 0.2) \times 10^8$ $L_\odot$, which is about two times higher than the upper limit estimated by Ouchi et al. (2013) and Ota et al. (2014). This tension can be explained by the fact that, not having *a priori* knowledge on the location and velocity of the [CII] emission, Ouchi et al. (2013) and Ota et al. (2014) extracted upper limits with arbitrary line widths and not taking into account fluctuations which may have been associated with a real signal. This issue may be common also to other [CII]

TABLE 1
ALMA DATA SUMMARY

dataset	t_{on} [h] (a)	antennae (b)	beam (c)	σ_{cont} [μJy] (d)	σ_{line} [μJy] (e)
2011.0.00115.S	3.2	25	$0.81''\times0.57''$	17	130
2012.1.00033.S	3.2	44	$0.28''\times0.22''$	11	98
combined	6.4	44	$0.39''\times0.31''$	9	88
combined and uv-tapered	6.4	44	$0.48''\times0.40''$	11	101

Notes: (a) On-source exposure time. (b) Number of antennae. (c) Angular resolution. (d) Sensitivity at λ_{rest} = 158 μm. (e) Sensitivity in a spectral channel of 100 km/s.

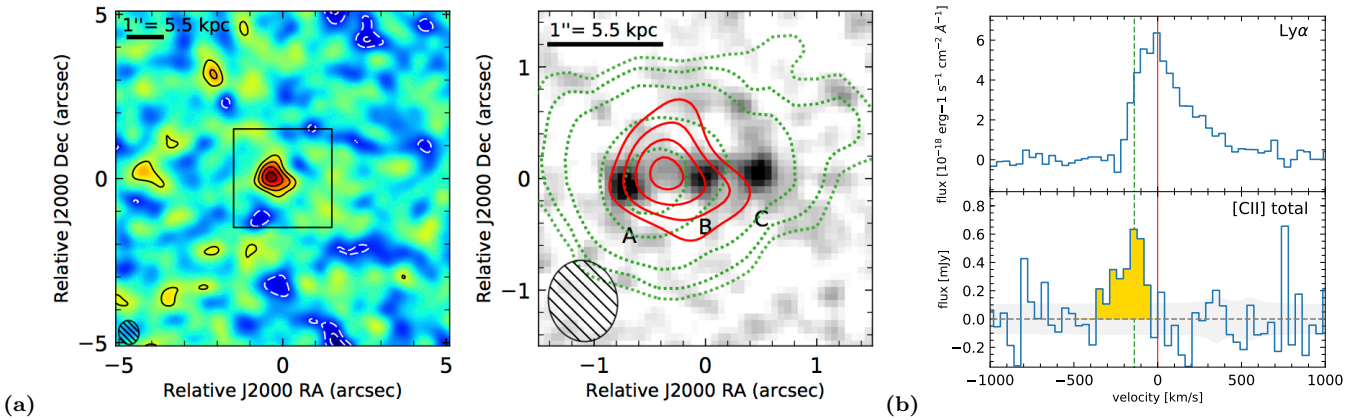

FIG. 1.— **(a)** The left panel shows the [CII] map of Himiko obtained by mean collapsing the uv-tapered cube over a velocity range between -320 and -50 km/s relative to the Lyα redshift, $z_{Ly\alpha} = 6.595$. Black(white) contours are shown in steps of $1\sigma = 70$ μJy/beam starting at $2(-2)\sigma$. The zoom of the central $3''\times3''$ around the location of the source is shown in the right panel: the grey background image shows the HST/WFC3 J_{125} observation, while the red contours indicate the [CII] emission with the same levels as in the left panel. Lyα intensity levels from Ouchi et al. (2013) are indicated with green contours. The ALMA beam is indicated the in bottom-left corners of both panels. **(b)** The top and bottom panels show the Lyα and [CII] spectra, respectively. The velocities are relative to $z_{Ly\alpha}$. The dashed green line indicates the velocity inferred from the [CII] profile. The grey shaded region indicates the 1σ error as a function of velocity.

non-detections in the literature, in the sense that some of the upper limits estimated in the past may be too low.

The measured [CII] luminosity is comparable to those measured in some other $z > 6$ star-forming galaxies with similar SFR_{UV}. In particular it is akin to the $L_{[CII]}$ observed in the CR7 (Matthee et al. 2017), which is a LAE with properties similar to Himiko (SFR=44 $M_\odot$/yr). In contrast to previous claims, our detection places Himiko along the local $L_{[CII]}$-SFR given by De Looze et al. (2014), as illustrated in Fig.2.

3.3. *Multi-component system*

Given the multi-clump shape of Himiko in the rest-frame UV images and the extended [CII] emission detected in the smoothed ALMA observations, we investigate the morphology of [CII] emission and its connection with the UV and Lyα counterparts.

A channel map analysis performed on the non-smoothed combined cube reveals that the extended [CII] emission is the result of two spectroscopically distinct components (hereafter $A_{[CII]}$ and $B_{[CII]}$) whose emission peak at two different locations of the system. Figure 3 shows the flux maps and spectra of the two components. The latter are extracted from an aperture as large as the beam and centred at the peak of the emission.

We identify the component $A_{[CII]}$ with a S/N=5 in the

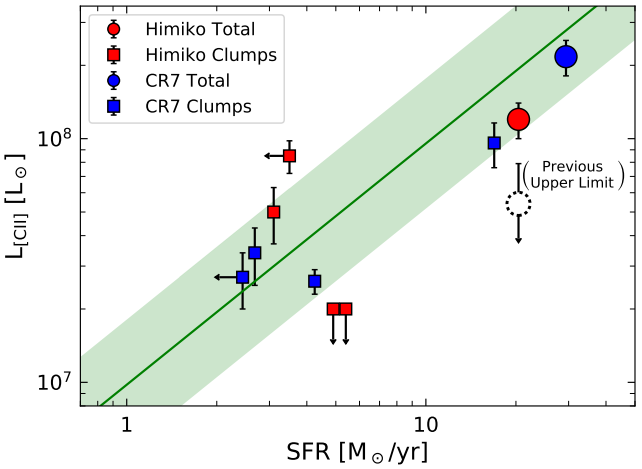

FIG. 2.— $L_{[CII]}$-SFR diagram. The green line shows the relations for local star-forming galaxies by De Looze et al. (2014). The location of Himiko's total emission is shown with the large red circle. The location of Himiko's subclumps is shown with red squares. We also report the location of CR7 and its subclumps. The dotted circle shows the previous [CII] upper limits for Himiko by Ouchi et al. (2013) and Ota et al. (2014)

channel map -100 km/s $< v < -365$ km/s. The cen-

TABLE 2
UV and far-IR properties of Himiko

	Himiko				
	Total	Clump A	$A_{[CII]}$ (Lyα peak)	Clump B ($B_{[CII]}$)	Clump C
RA [J2000]	-	2:17:57.61	2:17:57.59	2:17:57.57	2:17:57.53
DEC [J2000]	-	-5:08:44.96	-5:08:44.77	-5:08:44.87	-5:08:44.82
$z_{Ly\alpha}$	6.595	6.595	6.595	6.595	6.595
EW(Lyα) [Å]	78^{+8}_{-6}	68^{+14}_{-13}	> 68	3^{+20}_{-18}	6^{+12}_{-10}
J_{125}*	24.99 ± 0.08	26.54 ± 0.04	> 26.9	27.03 ± 0.07	26.43 ± 0.04
H_{160}*	24.99 ± 0.10	26.73 ± 0.06	> 27.3	27.04 ± 0.08	26.48 ± 0.05
SFR_{UV} [$M_\odot$/yr]*	20.4 ± 1.5	4.9 ± 0.2	< 3.5	3.1 ± 0.2	5.4 ± 0.2
$S_{158\mu m}$ [μJy]	< 27	< 27	< 27	< 27	< 27
L_{IR} [10^{10} $L_\odot$]†	< 3	< 3	< 3	< 3	< 3
SFR_{IR} [$M_\odot$/yr]	< 4	< 4	< 4	< 4	
$z_{[CII]}$	6.5913 ± 0.0004	-	6.5906 ± 0.0008	6.5915 ± 0.0003	-
$\Delta v_{Ly\alpha-[CII]}$ [km/s]	-145 ± 15	-	-175 ± 30	-140 ± 10	-
$FWHM_{[CII]}$ [km/s]	180 ± 50	-	240 ± 80	70 ± 20	-
$S_{[CII]}\Delta v$ [mJy km/s]‡	108 ± 13	< 26	73 ± 12	44 ± 8	< 26
$L_{[CII]}$ [10^8 $L_\odot$]‡	1.2 ± 0.2	< 0.2	0.85 ± 0.13	0.50 ± 0.10	< 0.2
[CII] size [kpc]	$(3.9 \pm 1.1) \times (1.7 \pm 1.1)$	-	$(3.7 \pm 0.6) \times (2.0 \pm 0.6)$	< 2	-

Note: * The magnitudes of A,B, and C are from Ouchi et al. (2013), while we perform $0.68'' \times 0.41''$ aperture photometry for $A_{[CII]}$. The latter is contaminated by the emission of clump A. The SFR_{UV} has been estimated from J_{125} flux by using Kennicutt & Evans (2012). † The L_{IR} estimates include the effect of the CMB (da Cunha et al. 2013; Ota et al. 2014). ‡ The upper limits on the [CII] emission are estimated by assuming a $FWHM = 100$ km/s.

troid of the emission is spatially offset by $\sim 0.2''$ toward the West relative to the UV position of the clump-A, but it is fully consistent with the peak of the extended Lyα nebula observed by Ouchi et al. (2013). We exclude that this [CII] component is directly associated with the UV clump A since the [CII] emission level at the location of the UV emission is $< 2\sigma$. As we will discuss later, positional offsets between UV and FIR line emission are not so rare in primeval galaxies (Maiolino et al. 2015; Willott et al. 2015; Carniani et al. 2017a). By fitting a 2D Gaussian profile to the channel map, we find that the [CII] emission of component $A_{[CII]}$ is spatially resolved with a beam-deconvolved size of $(0.68 \pm 0.10)'' \times (0.41 \pm 0.10)''$, which corresponds to a physical size of ~ 3.7 kpc. The [CII] profile peaks at -175 ± 30 km/s and has a line width of 240 ± 80 km/s. We measure $L_{[CII]} = (0.85 \pm 0.13) \times 10^8$ $L_\odot$ that corresponds to the $\sim$70% of the total [CII] luminosity inferred for Himiko.

The other component, $B_{[CII]}$, peaks at -175 ± 30 km/s and is narrower (FWHM $= 70 \pm 20$ km/s) than the former component. The knot of the [CII] emission is co-aligned with the UV clump-B, indicating that [CII] and UV emission arise from the same region. Since components $B_{[CII]}$ and $A_{[CII]}$ overlap in velocity, the flux map $B_{[CII]}$ shows also a tail emission associated with the $A_{[CII]}$ component. The core of the $B_{[CII]}$ emission is not spatially resolved indicating the the [CII] line is powered by a compact source with size < 2 kpc. We infer a [CII] luminosity $L_{[CII]} = (0.50 \pm 0.13) \times 10^8$ $L_\odot$.

Since around the $z_{Ly\alpha}$ we do not detect any emission close to the UV clumps A and C, we search for line emission in the ALMA cube between -1000 km/s and 1000 km/s relative to $z_{Ly\alpha}$. Only a putative detection is found at ~ -500 km/s and located at the UV position of the clump C. Because of the low significance (S/N=3.2), the emission can be spurious due to noise fluctuation, hence we consider it as a non detection. For the two UV clumps A and C, we therefore infer an upper limit on the [CII] luminosity $L_{[CII]} < 0.2 \times 10^8$ $L_\odot$ where we assume a line width of 100 km/s.

We note that while the [CII] emission in clump B(= $B_{[CII]}$) is consistent with the local $L_{[CII]}$–SFR relation, clumps A, C and $A_{[CII]}$ are scattered outside the local relation (Figure 2), as observed in other high-z galaxies (e.g. Maiolino et al. 2015).

Positional offsets between UV and [CII] emission observed both in the local and distant Universe may be ascribed to spatially distinct regions of the galaxy, and of their circumgalactic environment, characterised by different physical properties (e.g. Kapala et al. 2015; Croxall et al. 2017; Carniani et al. 2017a). For instance, the low [CII] luminosity at the location of the UV regions can be interpreted as a consequence of a local low metal content, but also in terms of strong feedback ionizing or expelling gas (Vallini et al. 2015; Katz et al. 2016; Olsen et al. 2017). Spatially-offset [CII] emission may also be explained in terms of dust obscuration and/or outflowing/inflowing gas. In the former scenario [CII] is excited in-situ by star-formation whose UV emission is heavily dust-obscured. In this context we note that Ouchi et al. (2013) infer a dust attenuation for Himiko of E(B-V)=0.15, which can hide a significant fraction of star forming regions traced by the UV emission. On the other hand, the spatially-offset [CII] can be associated to a satellite clumps in the process of accreting, or clumps expelled by galactic outflows; in these cases the [CII] emission is excited by the UV radiation of the closest star-formation region (e.g. clump A). This last scenario is also supported by the fact that Himiko re-

veals a triple major merger event whose extended Lyα nebula emission may be powered by both star formation and galactic winds (Ouchi et al. 2013; Zabl et al. 2015).

In summary UV and [CII] emission can trace different regions that should be treated as different subcomponents of the same system. A detailed discussion of multiple sub-components observed in $z > 5$ star-forming galaxies, as well as their offset relative to the star forming regions traced by the UV emission, is presented in a companion paper (Carniani et al. 2017b).

4. CONCLUSIONS

We have presented the analysis of archival ALMA data targeting the [CII] emission in the famous and luminous LAE Himiko, at $z = 6.595$. We have detected the FIR line with a level of significance of 9σ for the total, spatially integrated emission.

The measured luminosity of the line ($L_{[CII]} = 1.2 \times 10^8$ $L_\odot$) is fully consistent with the local $L_{[CII]}$-SFR relation, thereby mitigating the discrepancy with the local $L_{[CII]}$-SFR relation claimed in previous studies.

The ALMA data reveal that the [CII] profile is blueshifted by -145 km/s relative to the peak of Lyα, consistent with the fact that the asymmetric, blueward profile of Lyα is associated with absorption by the neutral intergalactic medium.

The [CII] emission is spatially resolved over $\sim$ 4 kpc and breaks into two sub-components. The location of the faintest [CII] component (which is spatially unresolved) is consistent with the UV emission of clump B, which is the central UV clump out of the three associated with Himiko. Instead, the brightest [CII] component is spatially extended (over 4 kpc) and its centroid is coincident with the peak of the Lyα nebula, and is spatially offset by $\sim 0.2''$ (=1kpc) relative to the nearest (and brightest) UV clump. While the [CII] luminosity of clump B is fully consistent with the local $L_{[CII]}$-SFR relation, all other clumps are scattered around the local relation, both above and below.

As already discussed in other works, the offsets between [CII] and UV emission, and the multi-clump nature of the [CII] emission, are likely associated with various effects, such as dust obscuration (preventing the detection of UV associated with [CII] emission), strong feedback (ionizing or removing gas in intense star forming regions), minor/major mergers and circumgalactic accreting/outflowing gas. A more extensive discussion of the multicomponent [CII] properties of high-z galaxies, their morphologies and offsets relative to the UV emission, is presented in a more extensive paper, discussing several more galaxies at $z > 5$, in a companion paper (Carniani et al. 2017b).

Finally, we note that the previous works had not detected the [CII] line in Himiko, giving an upper limit a factor of two lower than our detection. This is due to the difficulty of properly estimating the upper limit without prior knowledge about the location, redshift and width of the [CII] emission. This issue may affect also other past results; in particular, past upper limits on the [CII] emission in other high-z galaxies may be too low.

Acknowledgements. This paper makes use of the following ALMA data: ADS/JAO.ALMA#2011.0.00115.S and ADS/JAO.ALMA#2012.1.00033.S. ALMA is a partnership of ESO (representing its member states), NSF (USA) and NINS (Japan), together with NRC (Canada) and NSC and ASIAA (Taiwan), in cooperation with the Republic of Chile. The Joint ALMA Observatory is operated by ESO, AUI/NRAO and NAOJ. SC acknowledges support by the Science and Technology Facilities Council (STFC). RM and RA acknowledge support by the Science and Technology Facilities Council (STFC) and the ERC Advanced Grant 695671 "QUENCH".

REFERENCES

Bradač, M., Garcia-Appadoo, D., Huang, K.-H., et al. 2016, ArXiv e-prints, arXiv:1610.02099
Carniani, S., Maiolino, R., Pallottini, A., et al. 2017a, A&A, 605, A42
Carniani, S., Maiolino, R., Amorin, R., et al. 2017b, ArXiv e-prints, arXiv:1712.03985
Croxall, K. V., Smith, J. D., Pellegrini, E., et al. 2017, ApJ, 845, 96
da Cunha, E., Groves, B., Walter, F., et al. 2013, ApJ, 766, 13
De Looze, I., Cormier, D., Lebouteiller, V., et al. 2014, A&A, 568, A62
Díaz-Santos, T., Armus, L., Charmandaris, V., et al. 2013, ApJ, 774, 68
Gaia Collaboration, Brown, A. G. A., Vallenari, A., et al. 2016, A&A, 595, A2
Herrera-Camus, R., Bolatto, A. D., Wolfire, M. G., et al. 2015, ApJ, 800, 1
Inoue, A. K., Tamura, Y., Matsuo, H., et al. 2016, Science, 352, 1559
Kapala, M. J., Sandstrom, K., Groves, B., et al. 2015, ApJ, 798, 24
Katz, H., Kimm, T., Sijacki, D., & Haehnelt, M. 2016, ArXiv e-prints, arXiv:1612.01786
Kennicutt, R. C., & Evans, N. J. 2012, ARA&A, 50, 531
Knudsen, K. K., Richard, J., Kneib, J.-P., et al. 2016, ArXiv e-prints, arXiv:1603.02277
Lagache, G., Cousin, M., & Chatzikos, M. 2017, ArXiv e-prints, arXiv:1711.00798
Maiolino, R., Carniani, S., Fontana, A., et al. 2015, MNRAS, 452, 54
Matthee, J., Sobral, D., Boone, F., et al. 2017, ArXiv e-prints, arXiv:1709.06569
McMullin, J. P., Waters, B., Schiebel, D., Young, W., & Golap, K. 2007, in Astronomical Society of the Pacific Conference Series, Vol. 376, Astronomical Data Analysis Software and Systems XVI, ed. R. A. Shaw, F. Hill, & D. J. Bell, 127
Olsen, K., Greve, T. R., Narayanan, D., et al. 2017, ApJ, 846, 105
Ota, K., Walter, F., Ohta, K., et al. 2014, ApJ, 792, 34
Ouchi, M., Mobasher, B., Shimasaku, K., et al. 2009, ApJ, 706, 1136
Ouchi, M., Ellis, R., Ono, Y., et al. 2013, ApJ, 778, 102
Pallottini, A., Ferrara, A., Bovino, S., et al. 2017a, MNRAS, 471, 4128
Pallottini, A., Ferrara, A., Gallerani, S., et al. 2017b, MNRAS, 465, 2540
Pentericci, L., Carniani, S., Castellano, M., et al. 2016, ArXiv e-prints, arXiv:1608.08837
Schaerer, D., Boone, F., Jones, T., et al. 2015, A&A, 576, L2
Smit, R., Bouwens, R. J., Carniani, S., et al. 2017, ArXiv e-prints, arXiv:1706.04614
Smith, J. D. T., Croxall, K., Draine, B., et al. 2017, ApJ, 834, 5
Vallini, L., Gallerani, S., Ferrara, A., & Baek, S. 2013, MNRAS, 433, 1567
Vallini, L., Gallerani, S., Ferrara, A., Pallottini, A., & Yue, B. 2015, ApJ, 813, 36
Walter, F., Decarli, R., Carilli, C., et al. 2012, ApJ, 752, 93
Willott, C. J., Carilli, C. L., Wagg, J., & Wang, R. 2015, ApJ, 807, 180
Zabl, J., Nørgaard-Nielsen, H. U., Fynbo, J. P. U., et al. 2015, MNRAS, 451, 2050

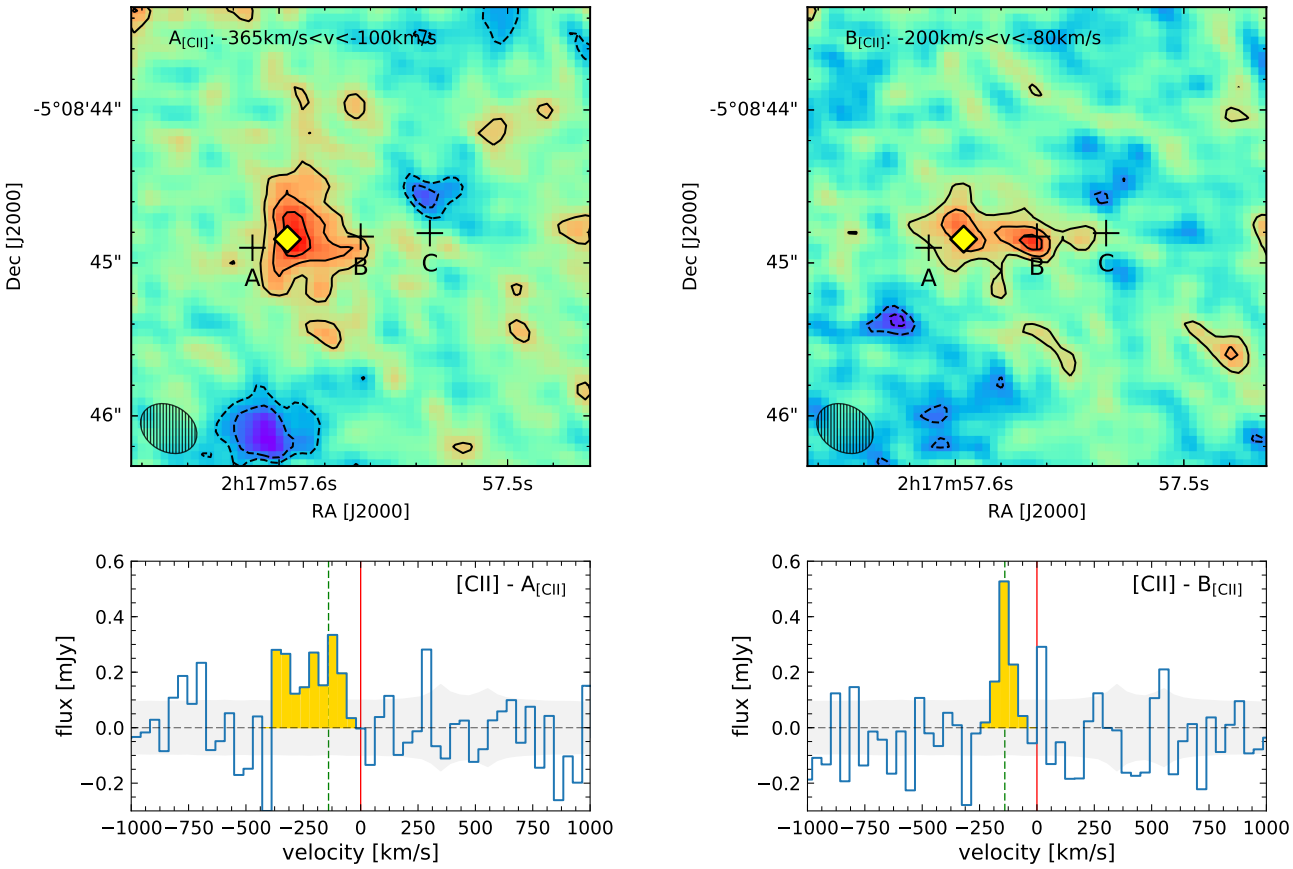

FIG. 3.— The top panels show the flux maps of the two [CII] components, clump $A_{[CII]}$ and $B_{[CII]}$. Contours show emission at levels of 2,3,4 and 5σ. The position of the three UV clumps is marked with black crosses, while the position of the Lyα peak is indicated with a yellow diamond. The bottom panels show the [CII] spectra of the two [CII] components. Velocities are relative to the peak of the Lyα peak (red line). The systemic velocity of the total [CII] profile is indicated with a red line.